

SlotMatch: Distilling Temporally Consistent Object-Centric Representations for Unsupervised Video Segmentation

Diana-Nicoleta Grigore^{1,*}, Neelu Madan^{2,*}, Andreas Møgelmo², Thomas B. Moeslund²,
Radu Tudor Ionescu^{1,◊}

¹University of Bucharest, Romania

²Aalborg University, Denmark

*Equal contribution. ◊Corresponding author: raducu.ionescu@gmail.com.

Abstract

Unsupervised video segmentation is a challenging computer vision task, especially due to the lack of supervisory signals coupled with the complexity of visual scenes. To overcome this challenge, state-of-the-art models based on slot attention often have to rely on large and computationally expensive neural architectures. To this end, we propose a simple knowledge distillation framework that effectively transfers object-centric representations to a lightweight student. The proposed framework, called SLOTMATCH, aligns corresponding teacher and student slots via the cosine similarity, requiring no additional distillation objectives or auxiliary supervision. The simplicity of SLOTMATCH is confirmed via theoretical and empirical evidence, both indicating that integrating additional losses is redundant. We conduct experiments on two datasets to compare the state-of-the-art teacher model, SLOTMATCH, with our distilled student. The results show that our student based on SLOTMATCH matches and even outperforms its teacher, while using $3.6\times$ less parameters and running $1.9\times$ faster. Moreover, our student surpasses previous unsupervised video segmentation models.

Code — <https://github.com/dianagrigoire/SlotMatch>

Introduction

A fundamental goal in machine perception is developing systems that, similarly to humans, understand complex visual scenes as compositions of distinct objects. This capability, studied in the area of *object-centric representation learning* (Burgess et al. 2019; Greff et al. 2019; Locatello et al. 2020) is a critical step for building agents that can reason about, interact with, and understand their surroundings.

Recent advances in self-supervised learning have produced powerful foundational models (Caron et al. 2021; He et al. 2022; Oquab et al. 2024). When integrated into slot-based attention frameworks (Kipf et al. 2022; Locatello et al. 2020), these models can discover and segment objects from complex scenes with remarkable fidelity. However, their success is predicated on their scale, as the high computational costs create bottlenecks for deployment. As such, typical self-supervised models are incompatible with resource-constrained environments, where object-centric representations built for video-related tasks would be most valuable.

Copyright © 2026, Association for the Advancement of Artificial Intelligence (www.aaai.org). All rights reserved.

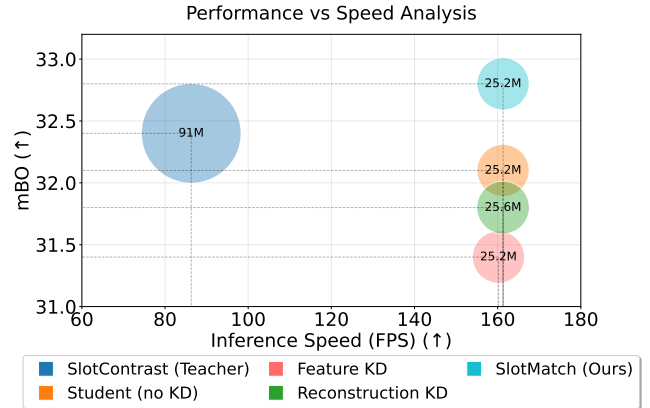


Figure 1: Comparison of SLOTMATCH (teacher) versus various student versions (including our SLOTMATCH), showing the trade-off between performance (mBO) vs. inference speed (FPS). Circle area indicates parameter count (in millions). SLOTMATCH (cyan) outperforms its teacher, while being nearly twice as fast. Best viewed in color.

To overcome this critical trade-off between performance and efficiency, we propose a knowledge distillation strategy tailored for object-centric models. Our method transfers the object discovery capabilities of a large *teacher* model to a lightweight *student*, aiming to create a final model that is not only more suitable for resource-constrained applications, but is also a more effective learner.

Our core contribution is a hybrid loss strategy that operates directly on the learned object slots. We frame the primary distillation objective as a direct matching loss, termed SLOTMATCH, where a slot from the student model serves as the “anchor” and the corresponding teacher slot provides the “positive” target. This pulls the student’s representation into alignment with the teacher’s proven semantic space. Crucially, the necessary repulsive force is not supplied by explicit negatives in the distillation loss itself. Instead, we rely on the student’s slot contrastive loss, which is concurrently optimized with the distillation objective. This combination effectively decomposes the learning signal: the distillation loss teaches each slot *what to be*, while the contrastive loss teaches it *not to be* a redundant copy of its other slots. We apply a similar principle to the reconstructed features, i.e. the

student is trained to minimize the mean squared error between its input and output representations, without distilling representations from the teacher. We provide theoretical and empirical evidence confirming that our simple distillation objective is sufficient and effective. More precisely, we show that distilling output features is redundant.

We carry out experiments on two benchmark datasets for unsupervised video segmentation, MOVi-E (Ghorbani et al. 2021) and YTVIS-2021 (Yang et al. 2021b). We compare our student based on SLOTMATCH with its state-of-the-art teacher, SLOTCONTRAST (Manasyan et al. 2025), as well as other competitive methods from recent literature (Aydemir, Xie, and Guney 2023; Kipf et al. 2022; Singh, Wu, and Ahn 2022; Zadaianchuk, Seitzer, and Martius 2023). The results indicate that our student outperforms all state-of-the-art models on both datasets. As shown in Figure 1, our student contains $3.6\times$ less parameters and runs $1.9\times$ faster than its teacher model, SLOTCONTRAST.

In summary, our contribution is threefold:

- We introduce SLOTMATCH, a knowledge distillation framework to distill slot attention by minimizing the cosine similarity between corresponding teacher and student slots.
- We provide theoretical evidence indicating that our slot distillation procedure can effectively distill information from the teacher, without requiring additional losses.
- We empirically show that our student based on SLOTMATCH is both effective and efficient, surpassing its teacher in terms of multiple performance metrics, while being $1.9\times$ faster and $3.6\times$ smaller.

Related Work

Object-centric representation learning. Unsupervised scene decomposition aims to discover object-based structure in raw perceptual inputs, without supervision. Early methods approached this task via perceptual grouping (Greff et al. 2016), spatial mixture models (Greff, Van Steenkiste, and Schmidhuber 2017), or foreground-background separation (Yang et al. 2021a). Recent approaches focused on *slot attention* (Locatello et al. 2020), which uses iterative attention to bind latent “slots” to individual objects. Since its introduction, the paradigm has been extended to incorporate real-world images (Seitzer et al. 2023), adaptive slot counts (Fan et al. 2024), and scale-invariant pipelines (Biza et al. 2023). While all of these have shown strong results in image-based object discovery, their adaptation to video requires additional mechanisms to ensure temporal consistency.

Object-centric video models. Slot attention was originally extended to video through methods such as SAVi (Kipf et al. 2022) and SAVi++ (Elsayed et al. 2022), which introduced cross-frame attention and optical flow to promote temporal coherence. Later, STEVE (Singh, Wu, and Ahn 2022) added sequential latent dynamics for video generation. VideoSAUR (Zadaianchuk, Seitzer, and Martius 2023) and SlotContrast (Manasyan et al. 2025) further enhanced the approach with contrastive objectives and stronger backbones, e.g. DINOv2 (Oquab et al. 2024). While effective,

these methods typically rely on compute-intensive encoders, limiting their applicability in real-time or embedded scenarios. Our work addresses this limitation by transferring object-centric knowledge from high-capacity video models to lightweight models via distillation.

Knowledge distillation. Knowledge distillation (KD) transfers information from a large “teacher” model to a compact “student” by aligning output distributions (Hinton, Vinyals, and Dean 2015), intermediate activations (Romero et al. 2014), or feature Jacobians (Czarnecki et al. 2017). Most of the existing KD studies are focused on traditional tasks (e.g. classification (Iordache, Alexe, and Ionescu 2025), language modeling (Gu et al. 2024)), with limited application to object-centric learning.

To the best of our knowledge, there are only a few recent papers that explore distillation from scene decomposition (Kara et al. 2024; Li et al. 2024; Liao et al. 2025; Seitzer et al. 2023). DIOD (Kara et al. 2024) introduced a self-distillation strategy in video slot attention, where an EMA teacher supervises the student by refining slot masks using optical flow and static cues. DINOSAUR (Seitzer et al. 2023) is a framework that distills high-level features from a pre-trained DINOv2 encoder by training a slot-based model to reconstruct them, enabling slot emergence on real-world images. Some works (Li et al. 2024) used slot attention to distill object-centric features from an image-based detector to an event-based one via slot-aware cross-modal alignment, while others proposed federated slot learning (Liao et al. 2025), using a teacher-student decoder setup to distill shared object-centric representations across distributed domains.

Nevertheless, none of the aforementioned studies considers structured slot-based representations. Our approach departs from standard distillation by aligning latent object slots directly, using a simple and effective cosine-based objective in the slot space. To our knowledge, SLOTMATCH is the first method to perform distillation at the level of semantic slot representations in video.

Method

We propose SLOTMATCH, a distillation framework designed to transfer temporally-consistent object-centric representations from a large teacher model to a compact student model. Our core insight is to operate directly in the slot space. As such, we introduce a novel similarity-based distillation objective that aligns semantic slot representations between teacher and student. Unlike standard methods, SLOTMATCH avoids conventional pixel-wise or feature-level distillation, instead relying on a direct semantic match between corresponding slots.

Problem setup. Let \mathbf{T} denote a frozen pre-trained teacher model with a high-capacity encoder, and \mathbf{S} denote a lightweight trainable student. Both operate on video frames and produce a fixed number of slot representations per frame, capturing object-centric semantics. Specifically, for a video frame \mathbf{x}_t , the teacher and student produce the slot representations defined below:

$$S_t^{\mathbf{T}} = \{s_{t,n}^{\mathbf{T}}\}_{n=1}^N \in \mathbb{R}^{N \times d}, S_t^{\mathbf{S}} = \{s_{t,n}^{\mathbf{S}}\}_{n=1}^N \in \mathbb{R}^{N \times d}, \quad (1)$$

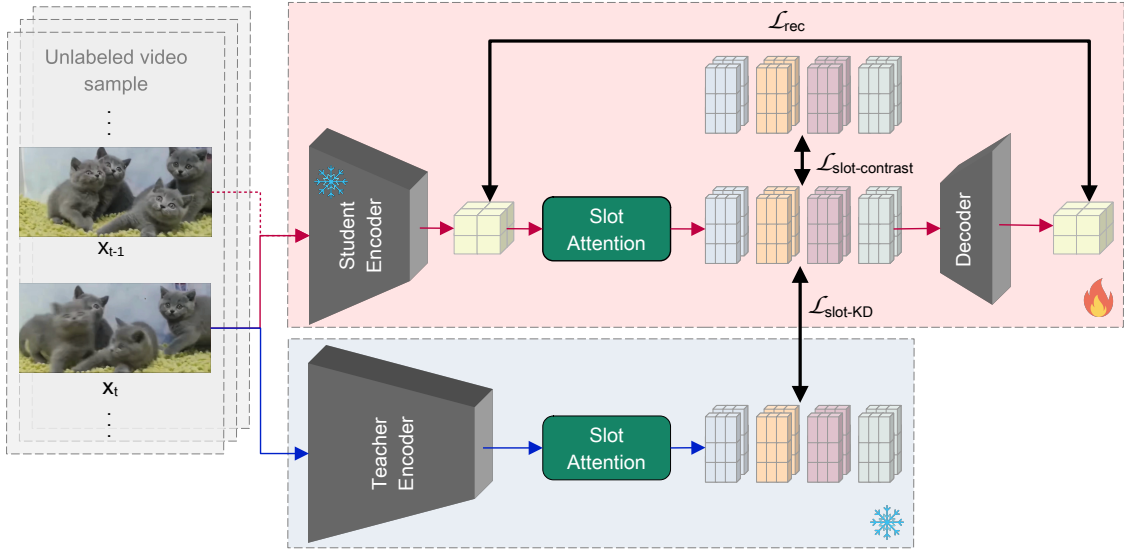


Figure 2: Our SLOTMATCH framework performs knowledge distillation from a large frozen teacher model to a compact trainable student model. Both models process video frames through slot attention mechanisms, with the student learning through three loss components: reconstruction (\mathcal{L}_{rec}), temporal consistency ($\mathcal{L}_{\text{slot-contrast}}$), and our novel slot matching loss ($\mathcal{L}_{\text{slot-KD}}$) that directly aligns corresponding slots between teacher and student using cosine similarity. Best viewed in color.

where each slot $s_{t,n} \in \mathbb{R}^d$ encodes information about a distinct object in the scene. We aim to train the student model such that its slots match the semantics of the teacher, preserve temporal consistency, and support scene reconstruction.

SLOTMATCH framework. In Figure 2, we showcase our SLOTMATCH framework, which operates in a dual-model fashion, with the teacher and student processing identical video inputs in parallel, through a slot-attention-based encoder-decoder architecture inspired by SlotContrast (Manasyan et al. 2025). First, a pre-trained DINOv2 (Oquab et al. 2024) backbone extracts spatial feature maps from each video frame. The teacher employs a higher-capacity encoder (e.g. ViT-B), while the student uses a lighter variant (e.g. ViT-S). Both encoders are frozen, but they contain a shallow trainable MLP that projects encoder features into a joint d -dimensional slot space. For each frame, we initialize a fixed number of slots N and iteratively update them via attention applied to encoded features. Slot attention compresses scene information into object-centric latent vectors. In the final part, the student employs a decoder that reconstructs the original features from slots. This ensures that slots are informative and can guide unsupervised segmentation. The teacher also uses a similar decoder during its training phase, but we do not employ its decoder in the distillation stage. To avoid clutter, we refrain from depicting the decoder of the teacher in Figure 2.

Training proceeds as formally described in Algorithm 1. For each mini-batch of B videos with T frames each, we extract per-frame slot representations $\mathbf{S}_{b,t}^{\mathbf{T}}$ and $\mathbf{S}_{b,t}^{\mathbf{S}}$ from the teacher and student models (steps 3–5), where b is the video index and t is the frame index. In step 7, a decoder reconstructs the input features from the student slots, producing $\hat{\mathbf{F}}_{b,t}^{\mathbf{S}}$. We next compute three loss terms: (i) a reconstruction

loss \mathcal{L}_{rec} that ensures the student slots retain sufficient scene-level information (step 8); (ii) a temporal contrastive loss $\mathcal{L}_{\text{slot-contrast}}$ that promotes both consistency and diversity of slots across adjacent frames (step 9); and (iii) our core distillation objective $\mathcal{L}_{\text{slot-KD}}$, which aligns each student slot with its teacher counterpart via cosine similarity (step 10). These are combined into a weighted loss (step 11) used to update the student parameters via gradient descent (step 12), while the teacher remains frozen during the whole process.

Slot-level distillation. In the teacher-student training phase, the first issue that arises is to find the correspondence between teacher and student slots, since the slots do not follow a precise order. We consider two options to determine the correspondence among teacher and student slots. One option is to perform explicit matching, e.g. via Hungarian assignment, while the other is to implicitly assume slot index correspondence, i.e. the n -th slot of the student corresponds to the n -th slot of the teacher. We ablate slot matching strategies in the supplementary and find negligible difference between matching and non-matching setups.

Each model produces N slot representations of dimension d , each of them encoding semantic information about a distinct object in the scene. The teacher model, through its larger encoder, learns robust object representations via its slots, capturing fine-grained semantic details, which we aim to distill into the student through direct slot alignment.

The core contribution of our method is the introduction of a novel cosine-based slot distillation loss $\mathcal{L}_{\text{slot-KD}}$ that aligns each student slot with its teacher counterpart:

$$\mathcal{L}_{\text{slot-KD}} = \frac{1}{B \cdot T \cdot N} \sum_{b=1}^B \sum_{t=1}^T \sum_{n=1}^N \left(1 - \frac{\langle s_{b,t,n}^{\mathbf{S}}, s_{b,t,n}^{\mathbf{T}} \rangle}{\|s_{b,t,n}^{\mathbf{S}}\| \cdot \|s_{b,t,n}^{\mathbf{T}}\|} \right), \quad (2)$$

where B is the mini-batch size, T is the number of frames

Algorithm 1: SLOTMATCH: Slot-Level Knowledge Distillation

Input: $\mathcal{D} = \{\mathbf{X}_1, \dots, \mathbf{X}_M\}$ – training set of M video sequences, each with T frames;
 $\mathbf{T} = \mathbf{T}^{\text{enc+attn+dec}}$ – pre-trained teacher model with frozen weights $\theta_{\mathbf{T}} = \{\theta_{\mathbf{T}}^{\text{enc}}, \theta_{\mathbf{T}}^{\text{attn}}, \theta_{\mathbf{T}}^{\text{dec}}\}$;
 $\mathbf{S} = \mathbf{S}^{\text{enc+attn+dec}}$ – student model with trainable weights $\theta_{\mathbf{S}} = \{\theta_{\mathbf{S}}^{\text{enc}}, \theta_{\mathbf{S}}^{\text{attn}}, \theta_{\mathbf{S}}^{\text{dec}}\}$;
 α – contrastive loss weight, β – slot distillation weight, η – learning rate; τ – temperature parameter;
 N – number of slots per frame; B – mini-batch size.
Output: $\theta_{\mathbf{S}}$ – learned weights of the student model.

```
1 repeat
2   foreach mini-batch  $\mathcal{B} = \{\mathbf{V}^{(b)}\}_{b=1}^B \subset \mathcal{D}$  do
3     foreach video index  $b \in \{1, \dots, B\}$  do
4       foreach frame index  $t \in \{1, \dots, T\}$  do
5          $\mathbf{S}_{b,t}^{\mathbf{T}} \leftarrow \mathbf{T}^{\text{enc+attn}}(\mathbf{x}_t^{(b)}; \theta_{\mathbf{T}}^{\text{enc}}, \theta_{\mathbf{T}}^{\text{attn}})$   $\triangleleft$  obtain teacher slots of shape  $N \times d$ 
6          $\mathbf{F}_{b,t}^{\mathbf{S}} \leftarrow \mathbf{S}^{\text{enc}}(\mathbf{x}_t^{(b)}; \theta_{\mathbf{S}}^{\text{enc}})$   $\triangleleft$  obtain student features
7          $\mathbf{S}_{b,t}^{\mathbf{S}} \leftarrow \mathbf{S}^{\text{attn}}(\mathbf{F}_{b,t}^{\mathbf{S}}; \theta_{\mathbf{S}}^{\text{attn}})$   $\triangleleft$  obtain student slots of shape  $N \times d$ 
8          $\hat{\mathbf{F}}_{b,t}^{\mathbf{S}} \leftarrow \mathbf{S}^{\text{dec}}(\mathbf{S}_{b,t}^{\mathbf{S}}; \theta_{\mathbf{S}}^{\text{dec}})$   $\triangleleft$  obtain decoded reconstruction
9          $\mathcal{L}_{\text{rec}} \leftarrow \frac{1}{B \cdot T} \sum_{b=1}^B \sum_{t=1}^T \|\hat{\mathbf{F}}_{b,t}^{\mathbf{S}} - \mathbf{F}_{b,t}^{\mathbf{S}}\|^2$   $\triangleleft$  feature reconstruction loss (based on MSE)
10         $\mathcal{L}_{\text{slot-contrast}} \leftarrow \frac{1}{B \cdot T \cdot N} \sum_{b=1}^B \sum_{t=1}^{T-1} \sum_{n=1}^N -\log \frac{\exp(\text{sim}(s_{b,t,n}^{\mathbf{S}}, s_{b,t+1,n}^{\mathbf{S}})/\tau)}{\sum_{b',t',n'} \exp(\text{sim}(s_{b,t,n}^{\mathbf{S}}, s_{b',t',n'}^{\mathbf{S}})/\tau)}$   $\triangleleft$  slot-slot contrastive loss
11         $\mathcal{L}_{\text{slot-KD}} \leftarrow \frac{1}{B \cdot T \cdot N} \sum_{b=1}^B \sum_{t=1}^T \sum_{n=1}^N \left(1 - \frac{\langle s_{b,t,n}^{\mathbf{S}}, s_{b,t,n}^{\mathbf{T}} \rangle}{\|s_{b,t,n}^{\mathbf{S}}\| \cdot \|s_{b,t,n}^{\mathbf{T}}\|}\right)$   $\triangleleft$  distillation loss (based on cosine similarity)
12         $\mathcal{L}_{\text{total}} \leftarrow \mathcal{L}_{\text{rec}} + \alpha \cdot \mathcal{L}_{\text{slot-contrast}} + \beta \cdot \mathcal{L}_{\text{slot-KD}}$   $\triangleleft$  compute combined training objective
13         $\theta_{\mathbf{S}} \leftarrow \theta_{\mathbf{S}} - \eta \cdot \nabla_{\theta_{\mathbf{S}}} \mathcal{L}_{\text{total}}$   $\triangleleft$  update the weights of the student model
14 until convergence;
```

in a video, and N is the number of slots. This formulation directly distills the object-centric latent space, promoting structured and efficient knowledge transfer. Each slot from the student is serving as an anchor that must align to its corresponding teacher slot as a positive, through cosine similarity-based optimization. Our formulation creates attractive forces that guide student representations toward the teacher’s semantic space.

Temporal and reconstruction losses. Following Manasyan et al. (2025), we integrate two auxiliary objectives to improve slot quality for the student, namely the slot-slot contrastive loss ($\mathcal{L}_{\text{slot-contrast}}$), and the feature reconstruction loss (\mathcal{L}_{rec}). This decomposition assigns distinct responsibilities to each loss component. Critically, the absence of explicit negative sampling in the distillation loss is compensated by the concurrent optimization of $\mathcal{L}_{\text{slot-contrast}}$, which provides the necessary repulsive forces to maintain slot distinctiveness for the student. While the slot distillation loss enforces semantic alignment between corresponding teacher-student slot pairs, the slot-slot contrastive loss maintains representational diversity among student slots, ensures temporal consistency by attracting slots representing the same object across consecutive frames, while also repelling slots from different objects within the mini-batch. The feature reconstruction loss \mathcal{L}_{rec} ensures that student slots contain sufficient information to reconstruct features given by the student

encoder, via its trainable decoder.

Overall training objective. The complete training objective integrates all three components:

$$\mathcal{L}_{\text{total}} = \mathcal{L}_{\text{rec}} + \alpha \cdot \mathcal{L}_{\text{slot-contrast}} + \beta \cdot \mathcal{L}_{\text{slot-KD}}, \quad (3)$$

where α and β control the relative importance of temporal consistency and knowledge transfer, respectively. The key advantages of our slot-based approach are its simplicity and efficiency. Unlike methods requiring complex assignment algorithms or feature-level matching, our direct correspondence assumption eliminates computational overhead, while maintaining effective knowledge transfer.

Theoretical justification. We conjecture that it is sufficient to employ the loss in Eq. (2) to perform effective knowledge distillation. In other words, we state that integrating additional losses, e.g. distilling the reconstructed features, is not necessary as long as $\mathcal{L}_{\text{slot-KD}}$ is minimized to zero after training. To support our conjecture, which simplifies the distillation framework, we introduce the following theorem:

Theorem 1. Let $s^{\mathbf{T}} \in \mathbb{R}^d$ be a teacher slot and $s^{\mathbf{S}} \in \mathbb{R}^d$ a student slot, with $\|s^{\mathbf{T}}\| = \|s^{\mathbf{S}}\| = r$, where $r > 0$. Let $f: \mathbb{R}^d \rightarrow \mathbb{R}^m$ be a K_f -Lipschitz neural network that decodes the slots into features. If the slot distillation loss converges

to a constant c , i.e.:

$$\mathcal{L}_{\text{slot-KD}}(s^{\mathbf{T}}, s^{\mathbf{S}}) = 1 - \frac{\langle s^{\mathbf{T}}, s^{\mathbf{S}} \rangle}{\|s^{\mathbf{T}}\| \cdot \|s^{\mathbf{S}}\|} = c, \quad (4)$$

then:

$$\mathcal{L}_{\text{rec-KD}}(f(s^{\mathbf{T}}), f(s^{\mathbf{S}})) = \|f(s^{\mathbf{T}}) - f(s^{\mathbf{S}})\|^2 \leq K \cdot c. \quad (5)$$

Proof. The proof is given in the supplementary. \square

The previous theorem indicates that if $c \rightarrow 0$, then the teacher-student reconstruction loss $\mathcal{L}_{\text{rec-KD}}$ is also converging to zero, which confirms our conjecture. In practice, the constant c might not approach zero, i.e. it might be hard to optimize $\mathcal{L}_{\text{slot-KD}}$ towards zero. In this case, introducing the teacher-student reconstruction loss into the optimization objective might be useful. We empirically test this objective and find that it does not help convergence to a better optimum. In summary, both theoretical and empirical evidence support our conjecture, suggesting that our simple knowledge distillation objective is sufficient.

Experiments

Datasets

We evaluate SLOTMATCH on both synthetic and real-world video datasets to assess its effectiveness across controlled, real-world and zero-shot scenarios.

MOVi-E. The Multi-Object Video (MOVi-E) dataset (Ghorbani et al. 2021) is generated using the Kubric simulator, which provides ground-truth object segmentation for precise evaluation. MOVi-E includes up to 23 objects per scene and is filmed with linear camera motion. The dataset includes complex object interactions, occlusions, and realistic textures, and the videos have a 24-frame length and a 256×256 resolution. We use the official train and validation splits, with 10,000 and 1,000 videos, respectively.

YTVIS-2021. To evaluate scalability to real-world scenarios, we use the YouTube Video Instance Segmentation 2021 (YTVIS-2021) dataset (Yang et al. 2021b). It contains unconstrained real-world videos, capturing diverse scenes including indoor/outdoor environments, multiple object categories, and complex interactions. Videos vary in length (up to 76 frames). The official split has 2,985 training videos and 1,421 validation ones, which we resize to 518×518 .

YTVIS-2021 \rightarrow OVIS. We conduct zero-shot experiments on Occluded Video Instance Segmentation (OVIS) (Qi et al. 2022), a dataset specifically focused on challenging scenarios. OVIS contains real-world videos with heavy occlusions, making it particularly suitable for testing temporal consistency when objects frequently disappear and reappear. The dataset features 607 training videos and 140 validation videos across 25 object categories.

Evaluation Metrics

We use two types of evaluation metrics, namely the Foreground Adjusted Rand Index (FG-ARI) and mean Best Overlap (mBO), and apply them at both image and video

levels. **FG-ARI** measures how well the model groups pixels belonging to the same object. With a range of 0 to 1, and a higher value indicating better performance, its focus is on *object discovery quality*, i.e. if the model correctly identifies which pixels belong to the same object. FG-ARI compares predicted object masks against ground-truth segmentation masks. **mBO** measures the spatial precision of object masks, i.e. how accurately the predicted masks align with ground-truth boundaries. For each predicted mask, it finds the ground-truth mask with the highest IoU, then averages the IoU across all objects. mBO focuses on *segmentation mask quality*, measuring how precise and well-defined the predicted object boundaries are.

For the image-level evaluation, we compute the FG-ARI and mBO metrics per frame, then average them. For video, we compute the metrics across entire video sequences, accounting for temporal consistency.

Baselines

We compare SLOTMATCH against a range of recent object-centric video segmentation models. These include slot-based methods such as SAVi (Kipf et al. 2022), STEVE (Singh, Wu, and Ahn 2022), SOLV (Aydemir, Xie, and Guney 2023), VideoSAUR (Zadaianchuk, Seitzer, and Martius 2023), and its DINOv2-enhanced variant, VideoSAURv2 (Manasyan et al. 2025). We reproduce the results of SLOTCONTRAST (Manasyan et al. 2025), which serves as the teacher in our framework based on knowledge distillation. We further introduce several new baselines, each employing a different distillation strategy, as follows:

- **Student (no KD)** is a SLOTCONTRAST model trained from scratch, using a smaller encoder version from the same family, namely DINOv2-small instead of DINOv2-base.
- **Feature KD** is a student model (based on DINOv2-small) which distills features from the frozen DINOv2-base teacher encoder. These are passed through a two-layer MLP, and the student is trained to match the transformed features via MSE.
- **Reconstruction KD** distills the reconstructed output of the teacher model to the student model, minimizing the MSE between the two outputs.

We also report results with various ablated versions or alternatives of SLOTMATCH, namely:

- **SLOTMATCH (MSE)** aligns teacher and student slot representations using MSE instead of cosine similarity.
- **SLOTMATCH + Reconstruction KD** combines slot-level distillation and reconstruction output distillation.
- **SLOTMATCH (predicted)** distills predicted slots (before slot attention) by minimizing cosine similarity.

Results

Quantitative results. In Table 1, we present comparative results on MOVi-E and YTVIS-2021. Remarkably, SLOTMATCH consistently outperforms all prior methods across both datasets, including its teacher, SLOTCONTRAST (Manasyan et al. 2025). Despite having $3.6 \times$ fewer parameters

Method	MOVi-E				YTVIS-2021			
	Image		Video		Image		Video	
	FG-ARI \uparrow	mBO \uparrow						
SAVi (Kipf et al. 2022)	-	-	42.8	16.0	-	-	-	-
STEVE (Singh, Wu, and Ahn 2022)	-	-	50.6	26.6	-	-	15.0	19.1
VideoSAUR (Zadaianchuk, Seitzer, and Martius 2023)	-	-	73.9	35.6	-	-	28.9	26.3
VideoSAURv2 (Manasyan et al. 2025)	-	-	77.1	34.4	-	-	31.2	29.7
SOLV (Aydemir, Xie, and Guney 2023)	80.8	-	-	-	-	-	-	-
SLOTCONTRAST (Manasyan et al. 2025) (teacher)	83.9	32.4	81.7	28.6	45.5	39.7	36.8	32.4
Student (no KD)	80.1	28.9	76.6	30.1	44.5	38.8	37.2	32.1
Feature KD	81.8	31.6	80.1	28.1	45.2	38.2	35.9	31.4
Reconstruction KD	81.4	31.5	81.1	29.1	44.9	38.8	35.6	31.8
SLOTMATCH (MSE)	82.1	30.2	78.6	26.4	45.1	39.7	36.9	32.6
SLOTMATCH + Reconstruction KD	74.4	29.7	66.2	24.1	45.6	38.3	36.1	31.1
SLOTMATCH (predicted)	83.9	31.9	81.8	28.5	44.9	39.7	37.3	32.8
SLOTMATCH	84.1	33.6	81.8	30.5	45.8	39.8	36.3	32.6

Table 1: Comparison of video object segmentation performance on MOVi-E and YTVIS-2021. We report FG-ARI and mBO scores at both image and video levels. SLOTMATCH outperforms all baselines and ablations. The best performance on each column is highlighted in bold.

Method	#Params (M) \downarrow	#GFLOPs \downarrow	Inference Time (ms) \uparrow
Teacher	91.0	8825.7	347.4
SLOTMATCH	25.2	3266.5	186.0
Reduction	3.61 \times	2.70 \times	1.87 \times

Table 2: Comparison of inference speed, number of parameters, and GFLOPs between the SLOTCONTRAST teacher and our SLOTMATCH student. Measurements are performed on an NVIDIA A100 with 40GB VRAM, using video samples from the YTVIS-2021 dataset.

and nearly $2\times$ faster inference speed than SLOTCONTRAST (as per Table 2), our student achieves higher mask precision (mBO) and comparable or better object separation (FG-ARI). Notably, we improve mBO on YTVIS from 32.4 to 32.8, while reducing latency by nearly half, demonstrating that accurate object-centric segmentation does not require large models.

We find that mBO improvements are most consistent on the real-world YTVIS dataset, where the teacher may overfit to slot assignment, but underperform on precise masks. Interestingly, our student avoids this overfitting and better balances separation and alignment. This aligns with our hypothesis that slot supervision can offer better generalization than end-to-end training with larger capacity alone.

Qualitative results. In Figure 3, we showcase qualitative comparisons of segmentation masks on challenging examples from MOVi-E and YTVIS. Our method produces sharper and more temporally-consistent masks than the student model without distillation. On MOVi-E, SLOTMATCH segments overlapping or partially occluded objects more cleanly, while on real-world YTVIS data, it shows improved boundary alignment and fewer slot collisions. These results highlight the benefit of slot-level supervision in guiding the student to focus on meaningful object structure.

Method	Image		Video	
	FG-ARI \uparrow	mBO \uparrow	FG-ARI \uparrow	mBO \uparrow
Student (no KD)	54.6	24.9	34.6	21.5
SLOTMATCH	55.8	25.5	34.8	21.5

Table 3: Zero-shot generalization results on the OVIS dataset, using models trained only on YTVIS. We compare the student trained from scratch (no KD) versus our SLOTMATCH student.

Method	β	Image		Video	
		FG-ARI \uparrow	mBO \uparrow	FG-ARI \uparrow	mBO \uparrow
Teacher	-	45.5	39.7	36.8	32.4
Student (no KD)	-	44.5	38.8	37.2	32.1
SLOTMATCH	0.1	44.5	39.1	34.9	32.5
	0.2	45.8	39.8	36.3	32.6
	0.3	44.4	39.1	36.3	32.5
	0.5	43.8	38.9	35.5	32.1
	0.8	43.9	38.3	35.4	32.0

Table 4: Ablation study on the YTVIS dataset showing the effect of varying the weight β of the distillation loss $\mathcal{L}_{\text{slot-KD}}$ in SLOTMATCH. The best performance across all metrics is achieved at $\beta = 0.2$.

Efficiency comparison. In addition to improving segmentation quality, SLOTMATCH significantly reduces computational cost compared to its teacher, SLOTCONTRAST. As shown in Table 2, our distilled student achieves a $3.6\times$ reduction in parameters (91M \rightarrow 25M), a $2.7\times$ reduction in FLOPs, and nearly $1.9\times$ higher inference speed on video sequences from YTVIS. We run our experiments on an NVIDIA A100 with 40GB VRAM. These gains come with no additional supervision and without sacrificing slot quality or temporal consistency. This highlights the practical benefits of our distillation approach in resource-constrained settings, enabling object-centric video understanding on

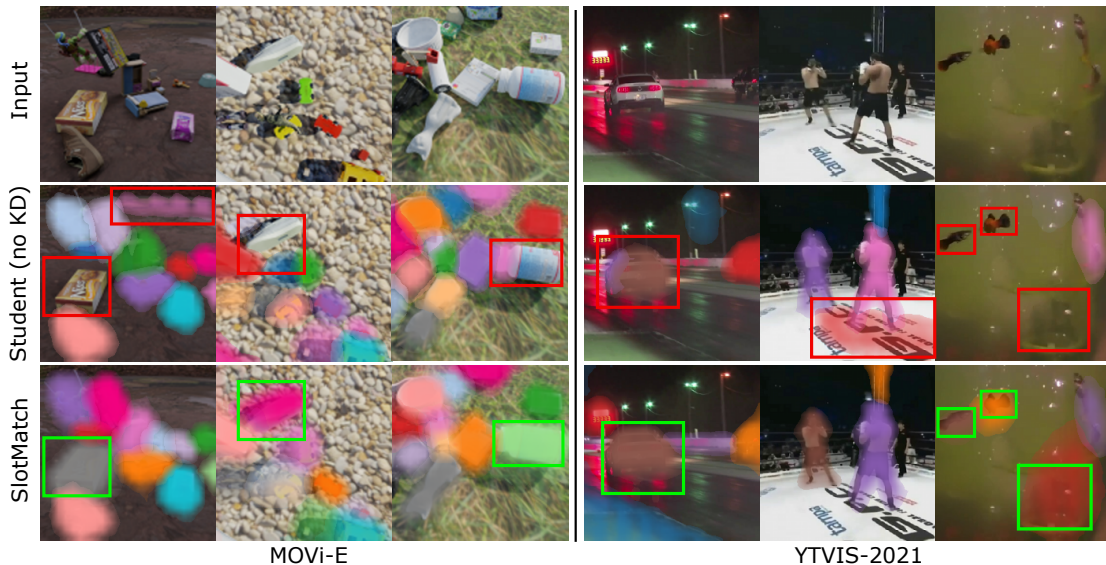


Figure 3: Qualitative comparison on MOVi-E (left) and YTVIS-2021 (right). The second row shows outputs from the student model, while the third row presents results from our distillation-based SLOTMATCH. Student errors, including missed slots, are marked in red. Corrections and additional slots introduced by SLOTMATCH are highlighted in green. Best viewed in color.

lightweight hardware.

Zero-shot generalization. In Table 3, we compare SLOTMATCH against the student trained from scratch (without distillation), in the zero-shot setup on the challenging OVIS dataset. Notably, SLOTMATCH maintains competitive video-level performance (FG-ARI: 34.8 vs. 34.6) compared with the student trained from scratch, while preserving slightly better spatial mask quality (mBO: 25.5 vs. 24.9). This demonstrates that distilling structured slot representations enhances robustness to occlusion and domain shift.

Ablation Studies

We conduct ablations to isolate the contribution of each component in our framework. The ablation results are summarized in Tables 1 and 4.

Slot vs. feature and reconstruction KD. To test whether slot representations are the best target for distillation, we compare our method with variants that distill encoder or decoder features via MSE (see Table 1). While feature KD and reconstruction KD bring modest gains over the student (no KD) baseline, they remain below our slot-based formulation, by significant margins. This supports our hypothesis that distilling structured object-centric representations leads to better temporal consistency and segmentation quality.

Cosine vs. MSE loss. We compare the proposed loss based on cosine similarity with an alternative loss based on MSE over slot representations. Cosine-based distillation yields more stable improvements across datasets, especially on YTVIS, likely due to its scale invariance and better alignment with semantic structure in high-dimensional spaces.

Matching predicted vs. corrected slots. Another ablation study targets the placement of our $\mathcal{L}_{\text{slot-KD}}$ loss, i.e. before or after slot attention. In general, it seems to be more beneficial

to apply the distillation to corrected slots, after slot attention. Yet, temporal consistency (measured at the video level) can be accurately ensured by distilling predicted slots, as confirmed by the results on YTVIS.

With or without reconstruction KD. To empirically determine if the proposed $\mathcal{L}_{\text{slot-KD}}$ loss is sufficient or not, we carry out experiments with an enhanced version of SLOTMATCH, where the distillation is also applied over reconstructed features via the $\mathcal{L}_{\text{rec-KD}}$ loss. Perhaps surprisingly, this double distillation procedure degrades performance by considerable margins on MOVi-E. The results show that adding additional distillation losses can make the distillation more complex and difficult to tune, eventually leading to inferior results. The empirical results only confirm Theorem 1, indicating that distillation via $\mathcal{L}_{\text{rec-KD}}$ is sufficient.

Distillation weight. We sweep the distillation loss weight β and observe best performance at $\beta = 0.2$ (see Table 4). Too little weight underutilizes the teacher signal, while too much harms diversity by forcing alignment too strongly.

Conclusions

In this work, we introduced SLOTMATCH, a simple and effective framework for distilling slot-based object representations from large teacher models into lightweight students. By aligning slots directly via cosine similarity, our method avoids auxiliary objectives. We showed both theoretically and empirically that this objective is sufficient to transfer semantic structure, leading to a student that outperforms its teacher in segmentation quality, while being significantly more efficient. Our results on MOVi-E and YTVIS established new state-of-the-art performance among unsupervised slot-based video models. In future work, we aim to continue our research in scaling down object-centric models for real-world deployment.

References

- Aydemir, G.; Xie, W.; and Guney, F. 2023. Self-supervised object-centric learning for videos. In *Proceedings of NeurIPS*, 32879–32899.
- Biza, O.; Van Steenkiste, S.; Sajjadi, M. S.; Elsayed, G. F.; Mahendran, A.; and Kipf, T. 2023. Invariant slot attention: object discovery with slot-centric reference frames. In *Proceedings of ICML*, 2507–2527.
- Burgess, C. P.; Matthey, L.; Watters, N.; Kabra, R.; Higgins, I.; Botvinick, M.; and Lerchner, A. 2019. MONet: Unsupervised Scene Decomposition and Representation. *arXiv preprint arXiv:1901.11390*.
- Caelles, S.; Pont-Tuset, J.; Perazzi, F.; Montes, A.; Maninis, K.-K.; and Van Gool, L. 2019. The 2019 DAVIS Challenge on VOS: Unsupervised Multi-Object Segmentation. *arXiv preprint arXiv:1905.00737*.
- Caron, M.; Touvron, H.; Misra, I.; Jégou, H.; Mairal, J.; Bojanowski, P.; and Joulin, A. 2021. Emerging properties in self-supervised vision transformers. In *Proceedings of ICCV*, 9650–9660.
- Czarnecki, W. M.; Osindero, S.; Jaderberg, M.; Swirszcz, G.; and Pascanu, R. 2017. Sobolev training for neural networks. In *Proceedings of NeurIPS*, 4281–4290.
- Elsayed, G.; Mahendran, A.; Van Steenkiste, S.; Greff, K.; Mozer, M. C.; and Kipf, T. 2022. SAVi++: Towards end-to-end object-centric learning from real-world videos. In *Proceedings of NeurIPS*, 28940–28954.
- Fan, K.; Bai, Z.; Xiao, T.; He, T.; Horn, M.; Fu, Y.; Locatello, F.; and Zhang, Z. 2024. Adaptive slot attention: Object discovery with dynamic slot number. In *Proceedings of CVPR*, 23062–23071.
- Ghorbani, S.; Mahdavian, K.; Thaler, A.; Kording, K.; Cook, D. J.; Blohm, G.; and Troje, N. F. 2021. MoVi: A large multi-purpose human motion and video dataset. *Plos one*, 16(6): e0253157.
- Greff, K.; Kaufman, R. L.; Kabra, R.; Watters, N.; Burgess, C.; Zoran, D.; Matthey, L.; Botvinick, M.; and Lerchner, A. 2019. Multi-object representation learning with iterative variational inference. In *Proceedings of ICML*, 2424–2433.
- Greff, K.; Rasmus, A.; Berglund, M.; Hao, T.; Valpola, H.; and Schmidhuber, J. 2016. Tagger: Deep unsupervised perceptual grouping. In *Proceedings of NeurIPS*.
- Greff, K.; Van Steenkiste, S.; and Schmidhuber, J. 2017. Neural expectation maximization. In *Proceedings of NeurIPS*, 6694–6704.
- Gu, Y.; Dong, L.; Wei, F.; and Huang, M. 2024. MiniLLM: Knowledge Distillation of Large Language Models. In *Proceedings of ICLR*.
- He, K.; Chen, X.; Xie, S.; Li, Y.; Dollár, P.; and Girshick, R. 2022. Masked autoencoders are scalable vision learners. In *Proceedings of CVPR*, 16000–16009.
- Hinton, G.; Vinyals, O.; and Dean, J. 2015. Distilling the knowledge in a neural network. *arXiv preprint arXiv:1503.02531*.
- Iordache, A.; Alexe, B.; and Ionescu, R. T. 2025. Multi-level feature distillation of joint teachers trained on distinct image datasets. In *Proceedings of WACV*, 7133–7142.
- Kara, S.; Ammar, H.; Denize, J.; Chabot, F.; and Pham, Q.-C. 2024. DIOD: Self-Distillation Meets Object Discovery. In *Proceedings of CVPR*, 3975–3985.
- Kipf, T.; Elsayed, G. F.; Mahendran, A.; Stone, A.; Sabour, S.; Heigold, G.; Jonschkowski, R.; Dosovitskiy, A.; and Greff, K. 2022. Conditional Object-Centric Learning from Video. In *Proceedings of ICLR*.
- Li, L.; Linger, A.; Millhaeusler, M.; Tsiminaki, V.; Li, Y.; and Dai, D. 2024. Object-centric cross-modal feature distillation for event-based object detection. In *Proceedings of ICRA*, 15440–15447.
- Liao, G.; Jogan, M.; Eaton, E.; and Hashimoto, D. A. 2025. FORLA: Federated Object-centric Representation Learning with Slot Attention. *arXiv preprint arXiv:2506.02964*.
- Locatello, F.; Weissenborn, D.; Unterthiner, T.; Mahendran, A.; Heigold, G.; Uszkoreit, J.; Dosovitskiy, A.; and Kipf, T. 2020. Object-centric learning with slot attention. In *Proceedings of NeurIPS*, 11525–11538.
- Manasyan, A.; Seitzer, M.; Radovic, F.; Martius, G.; and Zadaianchuk, A. 2025. Temporally consistent object-centric learning by contrasting slots. In *Proceedings of CVPR*, 5401–5411.
- Oquab, M.; Darcet, T.; Moutakanni, T.; Vo, H.; Szafraniec, M.; Khalidov, V.; Fernandez, P.; Haziza, D.; Massa, F.; El-Nouby, A.; et al. 2024. DINOv2: Learning robust visual features without supervision. *Transactions on Machine Learning Research*.
- Qi, J.; Gao, Y.; Hu, Y.; Wang, X.; Liu, X.; Bai, X.; Belongie, S.; Yuille, A.; Torr, P. H.; and Bai, S. 2022. Occluded Video Instance Segmentation: A benchmark. *International Journal of Computer Vision*, 130(8): 2022–2039.
- Romero, A.; Ballas, N.; Kahou, S. E.; Chassang, A.; Gatta, C.; and Bengio, Y. 2014. FitNets: Hints for Thin Deep Nets. *arXiv preprint arXiv:1412.6550*.
- Seitzer, M.; Horn, M.; Zadaianchuk, A.; Zietlow, D.; Xiao, T.; Simon-Gabriel, C.-J.; He, T.; Zhang, Z.; Schölkopf, B.; Brox, T.; et al. 2023. Bridging the gap to real-world object-centric learning. In *Proceedings of ICLR*.
- Singh, G.; Wu, Y.-F.; and Ahn, S. 2022. Simple unsupervised object-centric learning for complex and naturalistic videos. In *Proceedings of NeurIPS*, 18181–18196.
- Yang, C.; Lamdouar, H.; Lu, E.; Zisserman, A.; and Xie, W. 2021a. Self-supervised video object segmentation by motion grouping. In *Proceedings of ICCV*, 7177–7188.
- Yang, L.; Fan, Y.; Fu, Y.; and Xu, N. 2021b. The 3rd Large-scale Video Object Segmentation Challenge - video instance segmentation track.
- Zadaianchuk, A.; Seitzer, M.; and Martius, G. 2023. Object-centric learning for real-world videos by predicting temporal feature similarities. In *Proceedings of NeurIPS*, 61514–61545.

Supplementary

In the supplementary, we include the demonstration for Theorem 1, additional quantitative and qualitative results, reproducibility details, and the reproducibility checklist.

Theoretical Demonstration

We provide the proof of Theorem 1 below.

Proof. The cosine similarity between two (teacher and student) slots is defined as:

$$\cos \theta = \frac{\langle s^{\mathbf{T}}, s^{\mathbf{S}} \rangle}{\|s^{\mathbf{T}}\| \cdot \|s^{\mathbf{S}}\|}. \quad (6)$$

By replacing the definition in Eq. (6) in Eq. (4), we obtain the following:

$$\mathcal{L}_{\text{slot-KD}}(s^{\mathbf{T}}, s^{\mathbf{S}}) = 1 - \cos \theta = c, \quad (7)$$

which implies that:

$$\cos \theta = 1 - c. \quad (8)$$

We next express the sum of squared errors (squared Euclidean distance) between slots $\|s^{\mathbf{T}} - s^{\mathbf{S}}\|^2$ in terms of θ . We start from the following definition:

$$\|s^{\mathbf{T}} - s^{\mathbf{S}}\|^2 = \|s^{\mathbf{T}}\|^2 + \|s^{\mathbf{S}}\|^2 - 2 \cdot \langle s^{\mathbf{T}}, s^{\mathbf{S}} \rangle. \quad (9)$$

From Eq. (6), the scalar product between slots can be written as follows:

$$\langle s^{\mathbf{T}}, s^{\mathbf{S}} \rangle = \|s^{\mathbf{T}}\| \cdot \|s^{\mathbf{S}}\| \cdot \cos \theta. \quad (10)$$

Hence, Eq. (9) becomes:

$$\|s^{\mathbf{T}} - s^{\mathbf{S}}\|^2 = \|s^{\mathbf{T}}\|^2 + \|s^{\mathbf{S}}\|^2 - 2 \cdot \|s^{\mathbf{T}}\| \cdot \|s^{\mathbf{S}}\| \cdot \cos \theta. \quad (11)$$

By employing the following the assumption, specified in Theorem 1:

$$\|s^{\mathbf{T}}\| = \|s^{\mathbf{S}}\| = r, \quad (12)$$

we obtain:

$$\begin{aligned} \|s^{\mathbf{T}} - s^{\mathbf{S}}\|^2 &= 2 \cdot r^2 - 2 \cdot r^2 \cos \theta \\ &= 2 \cdot r^2 \cdot (1 - \cos \theta). \end{aligned} \quad (13)$$

By substituting Eq. (8) in Eq. (13), we obtain the following:

$$\|s^{\mathbf{T}} - s^{\mathbf{S}}\|^2 = 2 \cdot r^2 \cdot c. \quad (14)$$

The Lipschitz property of f gives us the following inequality:

$$\|f(s^{\mathbf{T}}) - f(s^{\mathbf{S}})\| \leq K_f \cdot \|s^{\mathbf{T}} - s^{\mathbf{S}}\|. \quad (15)$$

Squaring both sides leads to:

$$\|f(s^{\mathbf{T}}) - f(s^{\mathbf{S}})\|^2 \leq K_f^2 \cdot \|s^{\mathbf{T}} - s^{\mathbf{S}}\|^2. \quad (16)$$

Note that the left term in Eq. (16) is equal to $\mathcal{L}_{\text{rec-KD}}$, i.e.:

$$\mathcal{L}_{\text{rec-KD}}(f(s^{\mathbf{T}}), f(s^{\mathbf{S}})) \leq K_f^2 \cdot \|s^{\mathbf{T}} - s^{\mathbf{S}}\|^2 \quad (17)$$

We next substitute Eq. (14) inside Eq. (17) and obtain:

$$\mathcal{L}_{\text{rec-KD}}(f(s^{\mathbf{T}}), f(s^{\mathbf{S}})) \leq 2 \cdot K_f^2 \cdot r^2 \cdot c. \quad (18)$$

Let $K = 2 \cdot K_f^2 \cdot r^2$. Finally, we obtain:

$$\mathcal{L}_{\text{rec-KD}}(f(s^{\mathbf{T}}), f(s^{\mathbf{S}})) \leq K \cdot c, \quad (19)$$

which concludes the proof of Theorem 1. \square

Method	Image		Video	
	FG-ARI \uparrow	mBO \uparrow	FG-ARI \uparrow	mBO \uparrow
SLOTCONTRAST (Teacher)	89.1	12.1	73.3	11.8
Student (no KD)	93.7	11.9	76.6	11.6
SLOTMATCH (ours)	95.6	14.9	92.8	14.7

Table 5: Comparison of video object segmentation performance on DAVIS 2017. We report FG-ARI and mBO scores at both image and video levels.

Remarks:

- If the slots are normalized (i.e. $r = 1$), the bound simplifies to:

$$\mathcal{L}_{\text{rec-KD}}(f(s^{\mathbf{T}}), f(s^{\mathbf{S}})) \leq 2 \cdot K_f^2 \cdot c. \quad (20)$$

- In neural networks, the constant K_f depends on the weights and activations of the model, and it can be estimated via spectral norms.

Additional Results

Results on additional dataset. To further confirm that our framework generalizes to other datasets, we report additional results on the DAVIS 2017 dataset (Caelles et al. 2019). Our option is motivated by the fact that DAVIS contains high-quality annotations and challenging video sequences featuring complex object motion, occlusion, and dynamic backgrounds. DAVIS consists of short video clips with dense pixel-wise instance masks annotated per frame, making it particularly well-suited for evaluating fine-grained object-centric representations.

In Table 5, we compare SLOTMATCH with its SLOTCONTRAST teacher and a student that is trained from scratch (via SLOTCONTRAST without distillation), on the DAVIS dataset. The results further confirm the observations from the main article, namely that SLOTMATCH produces superior performance levels than the SLOTCONTRAST teacher, while also providing clear benefits over the student trained from scratch.

Ablation for Hungarian matching. As slots are inherently permutation-invariant, there is no guarantee for one-to-one alignment between student and teacher slots. This presents a challenge for direct knowledge transfer. To this end, we explore two matching strategies: (i) aligning slots by index positions (as proposed in the main article) or (ii) using the Hungarian algorithm to find the most similar slot pairs based on their features, before applying the loss. As shown in Table 6, distillation without Hungarian matching yields better performance in our setup, while also being more computationally efficient. A likely cause for this conclusion is that strict matching over-constrains the learning process, negatively impacting the convergence of the distillation model and leading to suboptimal results. Therefore, all results reported in the main paper omit the Hungarian matching step.

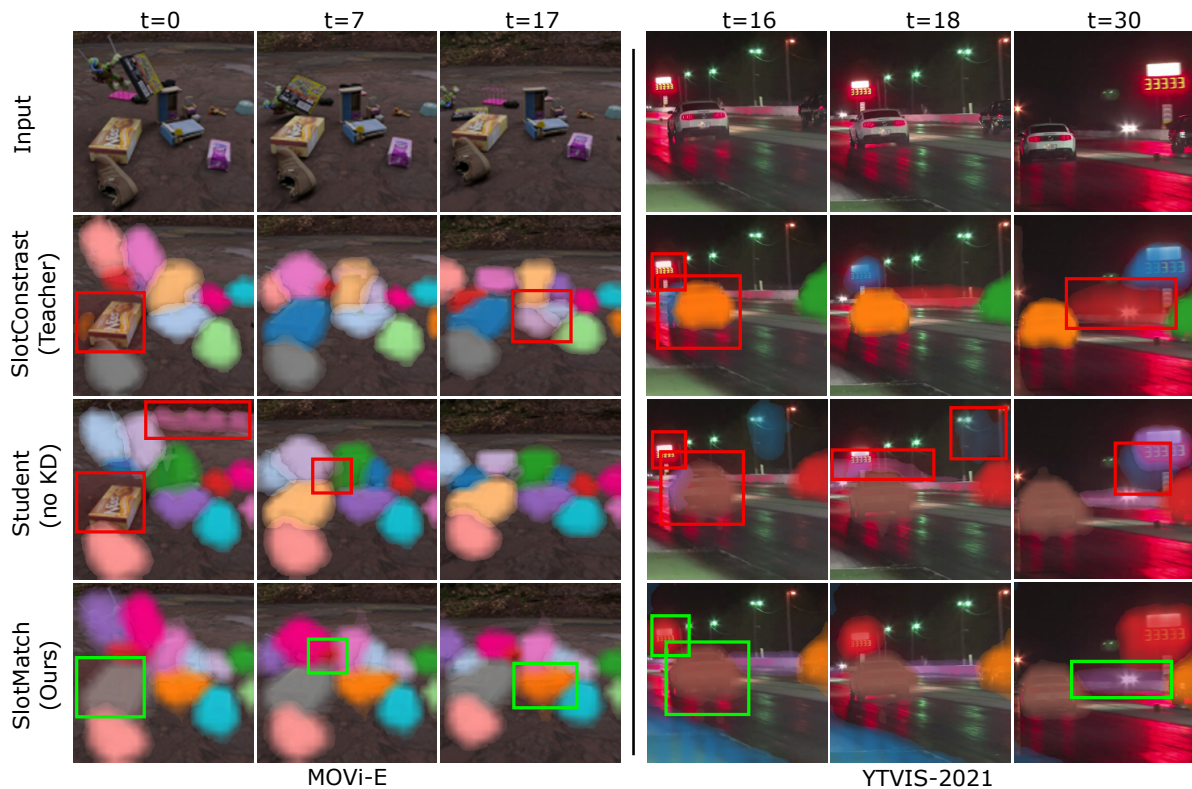


Figure 4: Qualitative segmentation results on MOVi-E (left) and YTVIS-2021 (right). The first row shows raw frames; the second and third rows show slots from the student and teacher models, respectively; the final row presents results from our distillation-based SLOTMATCH. SLOTMATCH recovers missed slots, refines object boundaries, and produces sharper, more consistent slots. Mistakes by the student and teacher models are annotated in red, while corrections and additional detections introduced by SLOTMATCH are highlighted in green. Best viewed in color.

Method	Image		Video	
	FG-ARI \uparrow	mBO \uparrow	FG-ARI \uparrow	mBO \uparrow
SLOTCONTRAST (Teacher)	83.9	32.4	81.7	28.6
Student (no KD)	80.1	28.9	76.6	30.1
SLOTMATCH (w/ matching)	83.5	31.8	81.5	28.6
SLOTMATCH (w/o matching)	84.1	33.6	81.8	30.5

Table 6: Comparison of distillation performance with and without Hungarian matching on the MOVi-E dataset. Omitting Hungarian matching (as proposed) leads to better performance.

Additional qualitative results. In Figure 4, we present a qualitative comparison of segmentation results produced by the teacher, student model trained without distillation, and our SLOTMATCH model, across MOVi-E (left-hand side) (Ghorbani et al. 2021) (left) and YTVIS-2021 (Yang et al. 2021b) (right-hand side).

On MOVi-E, which consists of synthetic scenes with numerous objects, both teacher and student models fail to detect certain objects in the initial video frames, e.g. the box on the left at $t = 0$. The teacher model suffers from over-clustering (e.g. object on the right at $t = 17$), fragmenting

single objects into multiple slots, while the student model (without distillation) fails to assign smaller or finer objects to any slot, e.g. the one in the center at $t = 7$. In contrast, our student trained with SLOTMATCH consistently recovers missed instances, resolves the over-clustering issue, produces robust slot representations, and maintains temporally consistent slot assignments, e.g. consistent coloring of objects from $t = 7$ to $t = 17$.

On YTVIS, a real-world and more challenging dataset with occlusions and poor lighting, we observe similar trends, i.e. both teacher and student models exhibit over-clustering in the initial frames, fragmenting single objects into multiple slots. In contrast, SLOTMATCH effectively refines the spatial extent of the masks and mitigates over-segmentation. Furthermore, our method outperforms in both slot assignment (e.g. correctly grouping the street light on the left) and boundary delineation (e.g. guardrail on the right).

Notably, green boxes indicate new or corrected slots introduced by our method, while red boxes highlight limitations of both the teacher and non-distilled student. These visual improvements confirm that distillation from the slots of a strong teacher not only preserves the original slot grouping, but also enhances the student’s robustness to occlusion, lighting variation, and clutter, all in an unsupervised fashion.

Hyperparameter	MOVi-E		YTVIS	
	Teacher	Student	Teacher	Student
Backbone	ViT-B/14	ViT-S/14	ViT-B/14	ViT-S/14
Feature size (m)	768	384	768	384
Slot dim (S)	128	128	64	64
#Slots (N)	15	15	7	7
Input size	336^2	336^2	518^2	518^2
#Patches	576	576	1369	1369
Batch size	16	16	64	64
Learning rate	0.0004	0.0004	0.0008	0.0008
Total steps	300K	300K	100K	100K
Loss weights	(1.0, 0.5)			
Slot attention iterations	2			
Contrastive temperature	0.1			
Gradient clip	0.05			
Predictor	Transformer (1×4)			

Table 7: Summary of key hyperparameters for all teacher and student models used in our experiments. All models use the same decoder, predictor, and loss weights.

Method	Dataset	Steps	GPU Hours
SLOTMATCH	MOVi-E	300K	≈ 138
	YTVIS	100K	≈ 39

Table 8: Approximate training time per experiment on two A100 GPUs.

Reproducibility Details

Model configurations. In Table 7, we provide a complete overview of model and training hyperparameters used across all experiments. The teacher and student models share a common slot attention architecture, decoder, and loss structure. For both datasets, the student differs by using a ViT-S/14 encoder with lower feature dimensionality. Other parameters such as slot count, learning rate, and contrastive loss temperature are held constant. These settings enable consistent and reproducible evaluation of our SLOTMATCH distillation approach.

Training time and compute resources. All experiments were conducted using two NVIDIA A100 GPUs (each with 40GB of VRAM). Training the student model on MOVi-E for 300K steps took approximately 138 hours. For YTVIS-2021, training required 39 hours for 100K steps. All models were implemented in PyTorch Lightning. Total GPU hours for each experiment are summarized in Table 8.

Random seeds and repeated runs. To evaluate the robustness of our method, all reported results are averaged across three runs using the following seeds: 42, 101 and 2048. Reported results in Table 9 reflect the average performance across these runs. In preliminary experiments, we found the standard deviation for FG-ARI, and mBO across seeds to be within ± 0.06 and ± 0.29 on YTVIS, indicating stable convergence behavior. All random seeds were set using PyTorch Lightning’s `seed_everything` function, as well as each independent module’s respective seed function, to ensure full reproducibility.

Run	Seed	Video FG-ARI \uparrow	Video mBO \uparrow
Run 1	42	36.2	32.9
Run 2	101	36.4	32.2
Run 3	2048	36.3	32.7
Mean	-	36.3	32.6
Std.	-	± 0.06	± 0.29

Table 9: Robustness evaluation of SLOTMATCH on the YTVIS dataset using three random seeds (42, 101, 2048). The last row reports the average performance across seeds. Consistent results across runs indicate stable training.

Data access and preprocessing. We used public benchmark datasets: MOVi-E (Ghorbani et al. 2021), YTVIS-2021 (Yang et al. 2021b), and OVIS (Qi et al. 2022). All datasets are publicly available and can be downloaded from the respective official repositories. Preprocessing for MOVi-E follows the original 336×336 center crop and normalization to $[-1, 1]$. For YTVIS, frames are resized using short-side resizing to 518 pixels with central cropping. OVIS is used for evaluation only. Temporal chunks of 4 frames are sampled per video for both training and evaluation. The corresponding preprocessing and data-related details are present in the configuration files.

Pretrained models and licensing. We will release pre-trained weights for both teacher and student models on MOVi-E and YTVIS in our code repository¹. Checkpoints will be provided with instructions for loading and evaluation. The code is released under the CC-BY-NC 4.0 license, and all dependencies are listed in the `environment.yml` file. The repository includes inference scripts, training pipelines, and evaluation tools for FG-ARI and mBO, along with an example configuration to reproduce results.

¹<https://github.com/dianagrigore/SlotMatch>